Backscattering properties and parametric model of Taihu Lake based on spectral classification

LU Chaoping, LV Heng, LI Yunmei

Key Laboratory of Virtual Geographic Environment Ministry of Education,
Nanjing Normal University, *Nanjing* 210046, *China*

Abstract: The parameters of backscattering coefficient model have significant temporal and spatial variability. In order to overcome this limit, a classification algorithm based on spectra dominant factors for Taihu Lake is established to classify the water reflectance spectra into three types. Quasi-analytical algorithm and optical closure are used in this paper to stimulate the backscattering coefficient for three types of water reflectance spectra in Taihu Lake according to the field measurement reflectance data. The properties of backscattering coefficient are also analyzed synchronously. On this basics, the backscattering coefficient parametric model for three types of water in Taihu Lake are established. As a result, the difference of the backscattering properties in different time and space is converted into the difference of bio-optical properties of dominant factor in water. Thus, the parametric models of backscattering coefficient are demonstrated to be suitable for different parts and different seasons of Taihu Lake.

Key words: Taihu Lake, spectral classification, Quasi-analytical algorithm, optical closure, backscattering coefficient
CLC number: X87 **Document code:** A

Citation format: Lu C P, Lv H and Li Y M. 2012. Backscattering properties and parametric model of Taihu Lake based on spectral classification. Journal of Remote Sensing, 16(2): 417–434

1 INTRODUCTION

Light-transfers in the water is influenced by the absorption and scattering of suspended solids, chlorophyll and colored dissolved organic matter (CDOM). Absorption coefficient and scattering coefficient are important inherent optical properties of waters. The back direction part of scattering light transmitted through the surface of water is the water-leaving radiance, which is the information source of water body detected by remote sensors and the important input parameter of bio-optics models (Forget, et al., 2001; Stramski, et al., 2004). So the backscattering characteristics of water body are the basis of bio-optics models.

Previous studies on backscattering properties of waters were relatively insufficient and most of them were focused on case 1 ocean waters, of which the optical properties is dominated by phytoplankton (Stramski, et al., 2001; Morel & Maritorena, 2001; Stramska, et al., 2003). Song, et al. (2006) conducted a study of the scattering properties in Huanghai Sea and East China Sea by the absorption and backscattering measured using 9 wavelength absorption and attenuation meter (AC9) and HydroScat-6. Sun, et al. (2007, 2008) carried out a study of the backscattering properties and its relationship with suspended solids using the data measured by absorption and attenuation spectra meter (AC-S) and Nine Wavelength Configurable Scattering Meter (bb9). Le, et al. (2009) simulated the backscattering by using radiative transfer theory. Ma, et al. (2008) estimated the backscattering probability of Lake Taihu waters. Huang (2009) analyzed the scattering characteristics and relevant factors in autumn Lake Taihu. Shi, et al. (2010) studied the depth profile of suspended particle scattering coefficient and its impact factors in Taihu Lake. The studies above indicated that the backscattering properties of coastal waters as well as lake waters have significant spatial and temporal differences. In other words, the backscattering coefficient is quite different both spatially and temporally. From the perspective of bio-optics, difference in reflectance spectra is caused by the different proportion of water components. So the differences of the optical properties in different time and space can be converted into the differences of biological properties by classifying the reflectance spectra, according to dominant factors in waters. As a result, water type should be identified in order to establish a union model for waters in different space and time.

In this paper, the specific objectives are: (1) to classify optically complex waters into different optical types by an algorithm based on reflectance shape and bio-optical characteristics; (2) to simulate the backscattering coefficient by calibrating quasi-analytical

Received: 2011-02-21; **Accepted:** 2011-04-18
Foundation: National Science Foundation for Young Scholars of China (No.40701136); National Natural Science Foundation of China (No.40971215); National Water Research and Demonstration of Remote Sensing System (No.2009ZX07527-006)
First author biography: LV Chaoping (1987—), male, master, he majors in GIS. E-mail: coollcp@126.com
Corresponding author biography: LV Heng (1977—), male, Ph.D., associate professor, his research interest is remote sensing of environment. He has published more than 10 papers. E-mail: HengLu@njnu.edu.cn

algorithm for each type of water; (3) to build parametric model of backscattering coefficient for each type of water; (4) to evaluate the accuracy of model for each type of water.

2 MATERIALS AND METHODS

The dataset contain 184 remote sensing reflectance measurements and water samples collected in Taihu Lake on November 2008, April 2009 and August 2010. Distribution of sample sites in Taihu Lake is shown in Fig. 1. Water samples and reflectance measurements were collected between 10:00 and 14:00 local time. Hyperspectral reflectance measurements were acquired by using ASD Field Spec Spectroradiometer. Surface water samples (2.5 L volume) were collected at a depth of 0.5 m below the surface water immediately after the reflectance measurement. The water samples were stored in a cooler with ice and placed in a dark location. Surface samples were filtered on Whatman GF/C and GF/F glass fiber filters and frozen for laboratory analyses of Chla, total suspended solids (TSS), and absorption coefficients at the end of the day.

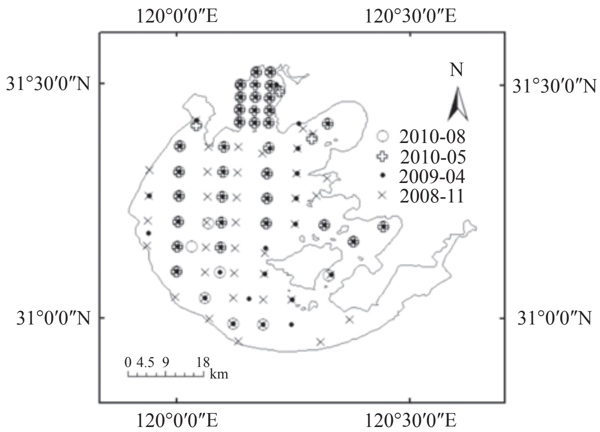

Fig. 1 Distribution of sample sites in Lake Taihu

2.1 Measurement of parameters

Hyperspectral reflectance measurements were recorded using an ASD Field Spec spectroradiometer. The method of collection and process is according to Tang, et al. (2004). With a field view of 25°, spectral radiance was measured at 2 nm intervals, ranging from 350 to 1050 nm. During the measurements, the instrument was held over the deck of an anchored ship approximately 1 m above water surface. Radiance was measured for the water surface, sky and a standard gray board. Ten curves were acquired for each target. In order to effectively avoid the interference of the ship with the water surface and the influence of direct solar radiation, the instrument was positioned at an angle of 90°—135° with the plane of the incident radiation away from the sun. The view of the water surface was controlled between 30° and 45° in the aplomb direction. In the calculation, the reflectance value of the sky light at air-water interface equals to 0.025; and the reflectance of the gray board has been accurately calibrated to 30%.

Chla extraction samples passed through GF/C filters (Whatman), after which Chla was extracted with 90% ethanol at 80℃ and spectrophotometrically analyzed at 750 and 665 nm. Absorption of suspended matter was measured using quantitative filter technique (QFT); absorption of CDOM was measured by cuvette. Concentration of suspended matter was measured by using the method according to Zhang, et al. (2007).

2.2 Spectral classification algorithm

According to the reflectance shape characteristics and corresponding biologic properties, waters in Taihu Lake were classified into three types: water dominated by phytoplanktonic suspended solids (Type A); by non-phytoplanktonic suspended solids (Type C) and by the both (Type B). Different types of reflectance are the reflection of different inherent optical-biological characteristics. For example, the valley at 675 nm in the reflectance curve is caused by the strong absorption of phytoplankton. Therefore, waters can be classified into three types dominated by different influence factors based on reflectance spectral classification.

In type A water, the absorption of pigment particles is strong while the scattering of suspended matter is relatively weak, so absorption peak at 675 nm and fluorescence peak at 700 nm present obviously in the reflectance spectra. In type C water, the characters of phytoplankton at 675 nm and 700 nm are covered by high concentration of suspended matter. And the reflectance peak at 570 nm is flatter than that in type A. Both characteristics of type A and type C are present in type B.

Through the statistic analysis of the slope of the left part of the peak around 570 nm, it was found that slope value of 0.00015 can be chosen to be one of criteria to identify type A from other two types. The absolute value of the slope between the reflectance at 675 nm and 700 nm can be another criterion to distinguish each type. Combining these two criteria, optically complex waters can be identified into three different types by using automatic classification algorithm (Fig. 2).

2.3 Backscattering and absorption simulation algorithm

Quasi-Analytical Algorithm (QAA) (Lee, et al., 2002) was pro-

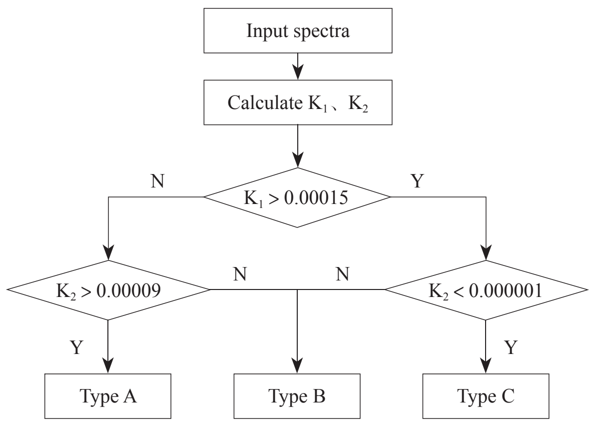

Fig. 2 Automatic search classification algorithm based on the reflectance spectra

Note: K_1=[peak($R_{rs}(\lambda_1)$)–$R_{rs}(\lambda_1$–40)]/40, (540<λ_1<600). K_1 is the slope of the left part of the peak around 570 nm;
K_2=[peak($R_{rs}(\lambda_2)$)–valley($R_{rs}(\lambda_3)$)]/(λ_2–λ_3), (670<λ_2<730, 620<λ_3<680). K_2 is the absolute value of the slope between the reflectance around 675 nm and 700 nm; peak() and valley() are the functions to search the position of peak and valley in given range.

posed to simulate the backscattering and absorption coefficient by inputting the above-surface remote sensing reflectance. The equation of reference wavelength λ_0 and corresponding absorption $a(\lambda_0)$ is empirical and not suitable for Taihu Lake. According to previous researches (Sun, et al., 2007; Sun, et al., 2008; Le, et al., 2009), the absorption of pure water after 700 nm is approximately equal to the total absorption of water in Taihu Lake. Therefore, the reference wavelength is obtained by iteration from 700 nm to 750 nm. Similarly, the exponent Y is obtained by iteration from 0 to 3. Value of g_0 and g_1 are set to 0.084 and 0.17, respectively, which are referred to the value in QAA. By using the optical closure principle (Tzortziou, et al., 2006) in the iteration simulation of QAA, the suitable reference wavelength and exponent will be identified. On this basis, the backscattering and absorption coefficient will be calculated. Detailed simulation process refers to algorithm 2 (Backscattering and absorption coefficient simulation algorithm).

Step 1 Set the initial value of reference wavelength λ_0 as 700 nm;

Step 2 Set the value of Y between 0 to 3 with the iteration step of 0.1, and calculate $b_{bp}(\lambda)$ and $a(\lambda)$ with the equations listed in Table 1;

Table 1 Steps and equations of semi-analytical algorithm

Step	Property	Equations	Approach
0	r_{rs}	$=R_{rs}/(0.52+1.7R_{rs})$	Semi-analytical
1	$u(\lambda)$	$=\frac{-g_0+[(g_0)^2+4g_1r_{rs}]^{1/2}}{2g_1}$	Semi-analytical
2	$a(\lambda_0)$	$=a_w(\lambda_0)$, λ_0 iterate from 700 nm to 730 nm	Iteration
3	$b_{bp}(\lambda_0)$	$=\frac{u(\lambda_0)a(\lambda_0)}{1-u(\lambda_0)}-b_{bw}(\lambda_0)$	Analytical
4	Y	Iterate from 0 to 3	Iteration
5	$b_{bp}(\lambda)$	$=b_{bp}(\lambda_0)\left[\frac{\lambda_0}{\lambda}\right]^Y$	Semi-analytical
6	$a(\lambda)$	$=\frac{[1-u(\lambda)][b_{bw}(\lambda)+b_{bp}(\lambda)]}{u(\lambda)}$	Analytical

Step 3 If the average relative error between simulated $a(\lambda)$ and measured $a(\lambda)$ is less than 10% (Tzortziou, et al., 2006), λ_0, Y, $b_{bp}(\lambda)$ and error will be recorded, or deleted as an outlier;

Step 4 If λ_0 is less than 750 nm, increase λ_0 by one, go back to **Step 2**; else go to **Step 5**;

Step 5 Calculate the mean value of error recorded in **Step 3** in accordance with λ_0, and choose the λ_0 with lowest mean value of error as the reference wavelength, and corresponding $b_{bp}(\lambda)$ as the simulation result.

3 RESULTS

3.1 Classified spectra

Algorithm 1 is applied to classify the measured reflectance spectra of Taihu Lake. Type A, B and C are shown in Fig. 3, Fig. 4 and Fig. 5, respectively. Type A represents water spectra dominated by phytoplankton; Type C represents water spectra dominated by non-phytoplanktonic suspended solids; Type B represents water spectra dominated by both. Fig. 6 shows the average value of each type of water spectra. Fig. 3, Fig. 4 and Fig. 5 show that each type of spectra has obvious characteristics. However, whether the types classified based on spectra are consistent with the bio-physics types

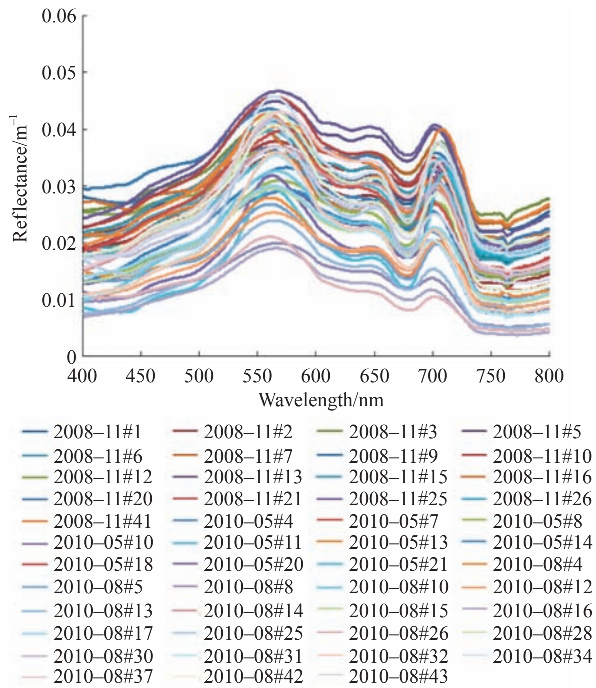

Fig. 3 Remote sensing reflectance Spectra of type A

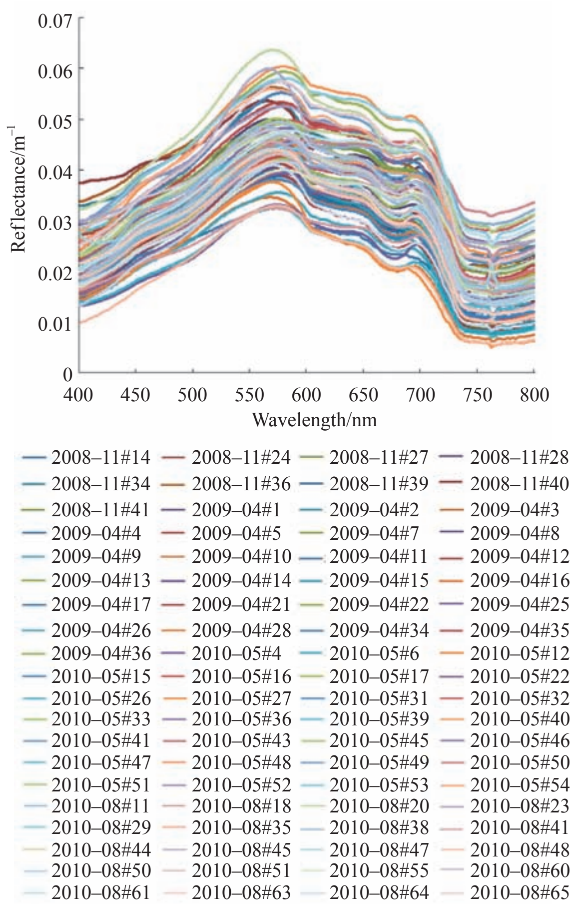

Fig. 4 Remote sensing reflectance Spectra of type B

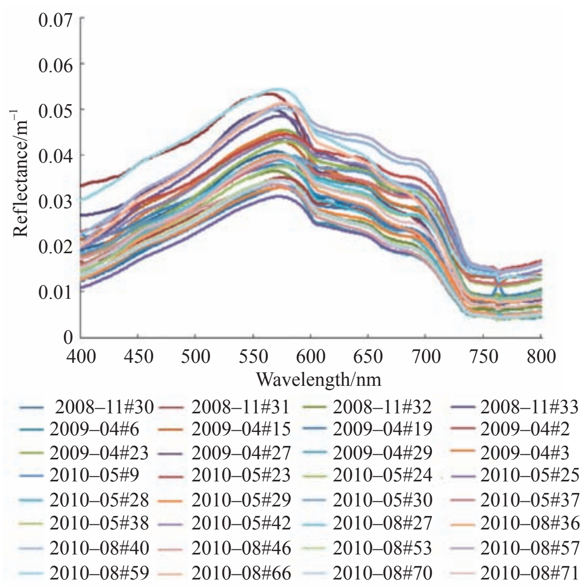

Fig. 5 Remote sensing reflectance spectra of type C

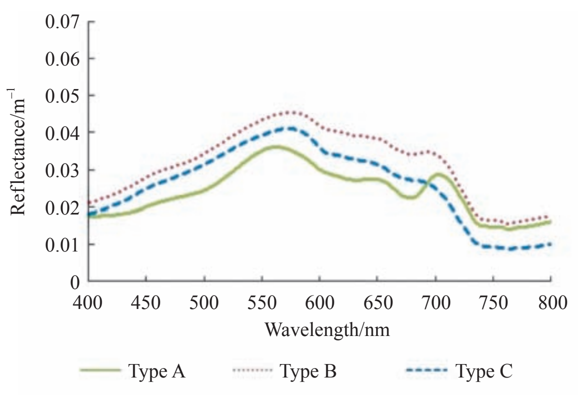

Fig. 6 Mean of the remote sensing reflectance spectra of 3 types

in real water is the key point of the classification algorithm.

Table 2 gives water constituent statistical parameters and its composition for corresponding types. A comprehensive description of three types is provided below.

Table 2 Statistical bio-optical parameters in different class waters

Parameters	Average value		
	Type A	Type B	Type C
TSM/(mg/L)	37.58	60.78	72.93
OSM/(mg/L)	16.47	10.27	11.25
ISM/(mg/L)	21.11	50.51	61.69
ISM/TSM	0.55	0.78	0.85
Chla/(mg/m^3)	44.06	17.14	8.08
aph(675)/(m^{-1})	0.88	0.35	0.21

Type A (Fig. 3, Fig. 6) has a lower reflectance value due to the absorption of phytoplankton. The valley around 675 nm is due to the strong absorption of pigment and the peak around 700 nm is due to the florescence of phytoplankton. This type has the highest levels of Chla with mean value of Chla 44.06 mg/m^3, which is 2 and 5 times of that in type 2 and type 3, respectively (Table 2). These samples are mainly distributed in Meiliang Bay and margins of Taihu Lake, where the water is dominated by phytoplankton.

Type C (Fig. 4, Fig. 6) has a higher reflectance value due to the scattering of suspended solids. The valley around 675 nm and the peak around 700 nm almost disappear due to the high concentration of suspended solids which covers the character of phytoplankton. The mean value of TSM and ISM are 72.93 mg/L and 61.69 mg/L, respectively. The concentration of TSM is not very high, but the ISM has a high proportion in TSM. The absorption of pigment at 675 nm is only quarter of that in type A. Type C contained 41 of the 184 samples, which distributed mainly in the center of Taihu Lake, where the water is dominated by suspended solids.

Type B (Fig. 5, Fig. 6) contains both features of Type A and C. The character of type A at 675 nm and 700 nm and the character of type C around 580 nm are both presented in type B. This type contains the middle level of TSM and Chla between type A and type C. The mean values of the two compositions are 60.78 mg/L and 17.14 mg/m^3, respectively.

3.2 Backscattering coefficients and their properties of three types

Algorithm 2 is applied to the classified reflectance to simulate the backscattering coefficient of each water type. The results indicate that the reference wavelength of type A, B and C are 715 nm, 710 nm, and type C is 706 nm, respectively. This result shows that the reference wavelength moves from long wave to short wave from type A to C.

Fig. 7, Fig. 8 and Fig. 9 show that the backscattering coefficient of each sample point has similar spectral features, which decays exponentially with the increase of wavelength. It is consistent with the arguments in previous reports (Sun, et al., 2008; Le, et al., 2009; Huang, et al., 2009). Backscattering coefficient value of each sample has some differences in one type, because the concentration of water component is different. Backscattering coefficient of each type are: type A, ranges from 0.32 m^{-1} to 3.31 m^{-1} with mean value of 1.54 m^{-1} at 400 nm; 0.22 m^{-1} to 1.65 m^{-1} with mean value of 0.74 m^{-1} at 532 nm; 0.18 m^{-1} to 0.77 m^{-1} with mean value of 0.47 m^{-1} at 532 nm. Type B, from 0.85 m^{-1} to 4.07 m^{-1}, 0.44 m^{-1} to 1.96 m^{-1}, 0.28 m^{-1} to 0.85 m^{-1}. Type C, 0.96 m^{-1} to 4.47 m^{-1}, 0.41 m^{-1} to 1.92 m^{-1}, 0.23 m^{-1} to 0.93 m^{-1}. Fig. 10 shows the mean values of three types of backscattering coefficients. The backscattering coefficient of type A is lower than other two types, especially from 400 nm to 600 nm. It is consistent with results of Morel (Morel, et al., 2006) that the backscattering coefficient of case 1 water which is dominated by phytoplanktonic suspended solids is lower than that of case 2 water, which is dominated by CDOM. And type A has a much gentler slope than type B and type C in the range of 400 nm to 600 nm.

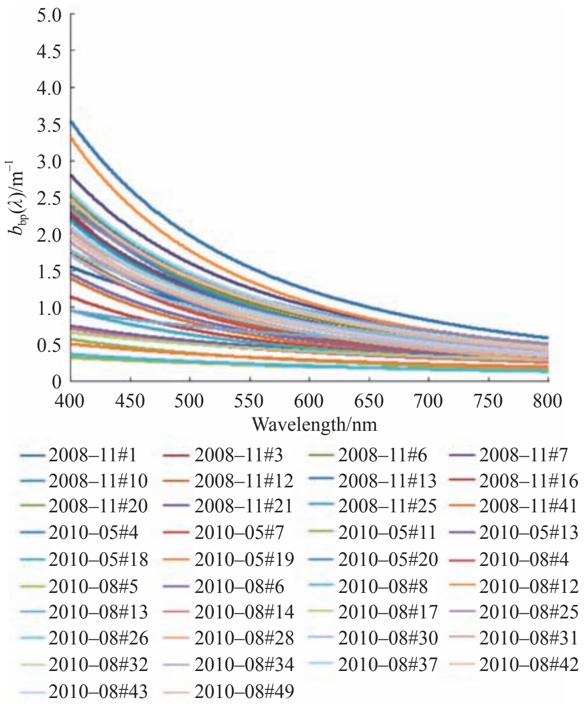

Fig. 7 Backscattering coefficient of type A

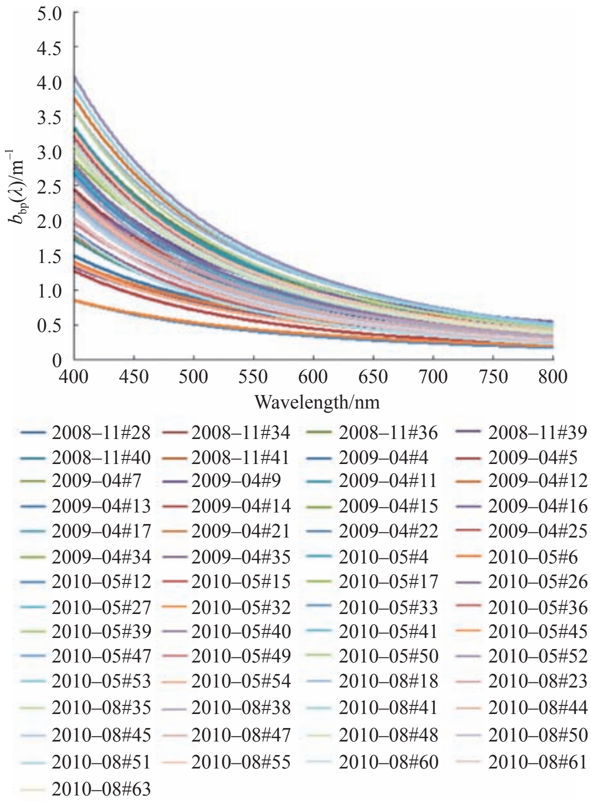

Fig. 8 Backscattering coefficient of type B

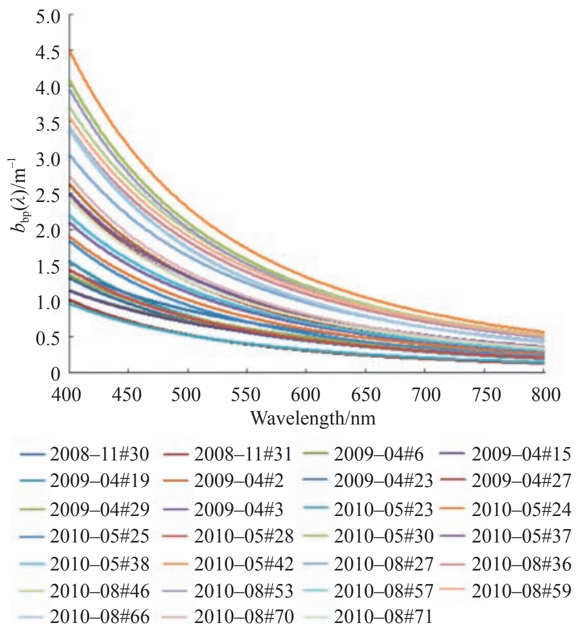

Fig. 9 Backscattering coefficient of type C

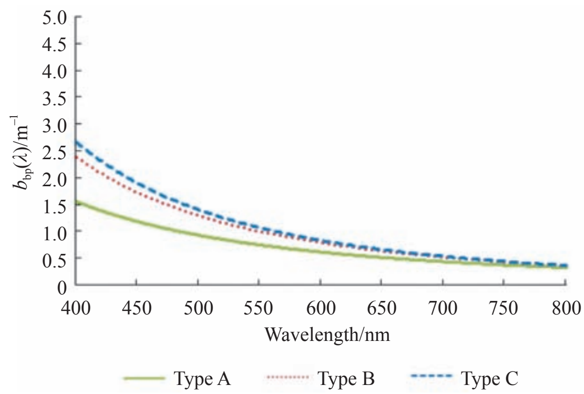

Fig. 10 Mean of backscattering coefficient for three types

3.3 The relationship between backscattering coefficient and suspended solids in different types

In order to find the influence of water components on backscattering, correlation analysis between backscattering coefficient and TSM, ISM, OSM and Chla were processed.

Type A water is dominated by phytoplankton, however, the proportion of ISM is still higher than OSM (Table 2). Therefore, the correlation coefficient between b_{bp} and ISM is higher than that between b_{bp} and OSM, and the highest between b_{bp} and OSM (Table 3). The correlation coefficient is highest between b_{bp} and OSM while lowest between b_{bp} and the rate of ISM and OSM. It indicates that type B water is dominated by both phytoplankton and suspended solids. The correlation coefficient between b_{bp} and ISM is highest in type C water.

Table 3 Correlations between backscattering coefficient and water component concentrations

	TSM	ISM	OSM	Chla	ISM/TSM
b_{bp}(532) of type A	0.76	0.56	0.48	0.53	0.38
b_{bp}(532) of type B	0.80	0.65	0.37	0.21	0.19
b_{bp}(532) of type C	0.77	0.89	0.65	0.24	0.63

Linear functions were applied to fit with the backscattering coefficient and TSM/ISM. As is shown in Fig. 11, Fig. 12, Fig. 13, the b_{bp} of type C has the best fitness with ISM, while the b_{bp} of type A has the lower correlation with TSM. Regression equations of each type are listed as below.

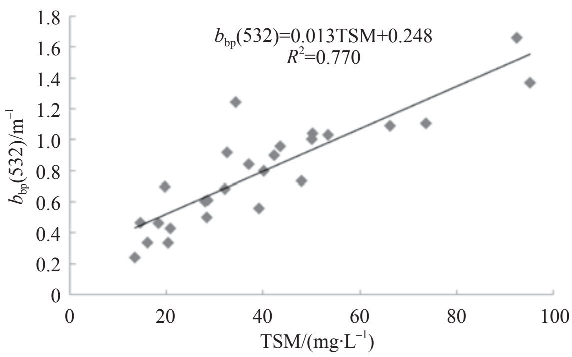

Fig. 11 Curve fitting of b_{bp}(532) and TMS for type A water

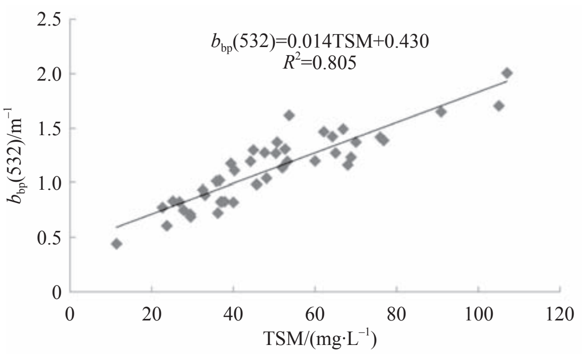

Fig. 12 Curve fitting of b_{bp}(532) and TMS for type B water

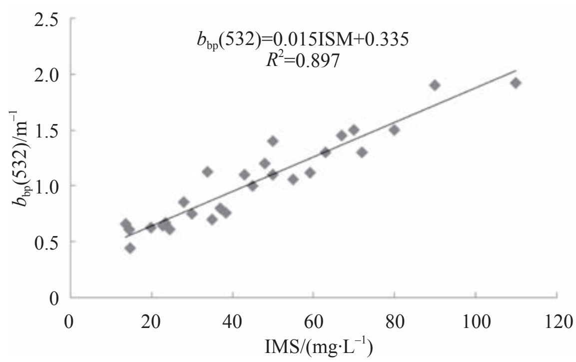

Fig. 13 Curve fitting of b_{bp}(532) and IMS for type C water

Type A: $b_{bp}(532)=0.013\times TSM+0.248$ (1)

Type B: $b_{bp}(532)=0.014\times TSM+0.430$ (2)

Type C: $b_{bp}(532)=0.015\times ISM+0.335$ (3)

3.4 Parametric models of backscattering coefficient

In order to obtain the backscattering coefficient of whole wavelength, parametric models of backscattering coefficient were built by using b_{bp} of certain wavelength. At present, the normal model to parameterize b_{bp} is an exponential function (Stramska, et al., 2003; Song, et al., 2006).

$$b_{bp}(\lambda)=b_{bp}(\lambda_0)\left[\frac{\lambda_0}{\lambda}\right]^n \quad (4)$$

where $b_{bp}(\lambda_0)$ is the backscattering coefficient at reference wavelength λ_0, n is the exponential index, which is affected by the concentration and composition of suspended solids.

In this paper, 532 nm is used as the reference wavelength to parameterize backscattering coefficient for three type of water, respectively. The process can be divided into two steps. First step is to regress $b_{bp}(\lambda)$ and $b_{bp}(532)$ by using linear function of $b_{bp}(\lambda)=A(\lambda)\times b_{bp}(532)$; a second step is to regress A and the ratio of λ_0 and λ using exponent function. The results show that the indices n of type A, B, C are 2.12, 2.51 and 2.69, respectively. Finally, parametric models of backscattering coefficient are built, which are shown as Eq. (5), Eq. (6) and Eq. (7).

Type A: $$b_{bp}(\lambda)=b_{bp}(532)\left[\frac{532}{\lambda}\right]^{2.12} \quad (5)$$

Type B: $$b_{bp}(\lambda)=b_{bp}(532)\left[\frac{532}{\lambda}\right]^{2.51} \quad (6)$$

Type C: $$b_{bp}(\lambda)=b_{bp}(532)\left[\frac{532}{\lambda}\right]^{2.69} \quad (7)$$

Replace $b_{bp}(532)$ in Eq. (5), Eq. (6) and Eq. (7) with Eq. (1), Eq. (2) and Eq. (3), there will be Eq. (8), Eq. (9) and Eq. (10).

Type A: $$b_{bp}(\lambda)=(0.013\times TSM+0.248)\left[\frac{532}{\lambda}\right]^{2.12} \quad (8)$$

Type B: $$b_{\text{bp}}(\lambda) = (0.014 \times \text{TSM} + 0.430)\left[\frac{532}{\lambda}\right]^{2.51} \quad (9)$$

Type C: $$b_{\text{bp}}(\lambda) = (0.015 \times \text{ISM} + 0.335)\left[\frac{532}{\lambda}\right]^{2.69} \quad (10)$$

Several scholars studied the parametric models of backscattering coefficient. However, the exponential index presented large diversity. Song (Song & Tang, 2006) obtained the exponential index ranges from 0.61 to 1.99 with an average value of 1.146 in the study of the scattering properties in Huanghai Sea and East China Sea. Sun (Sun, et al., 2007) found that the exponential index of Taihu Lake was 3.06, by using the measuring instruments AC-S and b_{bp}. Le (Le, et al., 2009) obtained the exponent index of Taihu Lake ranges from 1.32 to 2.8 with an average value of 2.09 through the radiative transfer simulation. It can be seen from the above that the exponential index of Taihu Lake varies in different seasons and areas due to the temporal and spatial variation of water composition in Taihu Lake. Taihu Lake is a typical large shallow lake. So its hydrodynamic environment, external environment and other factors lead to the uncertainty of water optical properties (Zhang, et al., 2005).

The exponential index for three water types in this paper are within the range from 2.09 (Le, et al., 2009) to 3.06 (Sun, et al., 2007), and the exponential index of type A is closer to Le (Le, et al., 2009), while the exponential index of type C is closer to Sun (Sun, et al., 2008). This precisely illustrates that backscattering coefficient simulation based on the classification can overcome the parameter fluctuations in parametric model caused by time and space difference and external factors.

3.5 Accuracy assessment

Absorption coefficient is calculated from backscattering coefficient by Quasi-analytical algorithm. Considering that there is no b_{bp} measurement, absorption coefficient is chosen to assess the accuracy of models. Algorithm 2 was used to calculate absorption coefficient with the input of classified dataset and original dataset, respectively. As is shown in Table 4, the average relative error of classified data is 38% less than unclassified.

Table 4 Comparison of the simulation results between the classified data and original data

	Reference wavelength λ_0			Average relative error/%			Y		
original	710			11.7			2.54		
classified	Type A	Type B	Type C	Type A	Type B	Type C	Type A	Type B	Type C
	715	710	706	6.5	7.3	6.1	2.12	2.51	2.69

4 CONCLUSION

In order to overcome the parameter fluctuations in parametric model caused by time and space difference, a classification algorithm based on spectra dominant factors for Taihu Lake was used to classify the reflectance spectra into three types, such as water spectra dominated by phytoplanktonic suspended solids, non-phytoplanktonic suspended solids and both. Then, quasi-analytical algorithm and optical closure were applied to stimulate the backscattering coefficient for three types of water in Taihu Lake. Finally, the parametric models of backscattering coefficient for three types of water were established. Consequently, the differences of the backscattering properties in different time and space were converted into the differences of bio-optical properties of dominant factor in water. The parametric models of backscattering coefficient are suitable for different areas and different seasons of Taihu Lake.

(1) A classification algorithm based on spectra characteristics was used to classify the reflectance spectra into three types, such as water spectra dominated by phytoplanktonic suspended solids, by non-phytoplanktonic suspended solids and by the both. By comparing the types classified based on spectra and on bio-physics, it has shown that the classification algorithm has good effect in distinguishing water types.

(2) Lee (Lee, et al., 2002) indicated that the reference wavelength moves to long wave as the water become more turbid. However, the error of reflectance becomes larger as the wave goes longer. In this paper, considering the absorption of water around 715 nm is nearly equal to the absorption of pure water, range of 700 nm to 730 nm was used to iterate to find the best wavelength for each type. The result showed that 715 nm, 710 nm, 706 nm were suitable for type A, type B and type C, respectively.

(3) Wavelength of 532 nm was used to parameterize the backscattering coefficient models. The exponent indices of type A, type B, type C were 2.12, 2.51 and 2.69, respectively.

(4) Accuracy of classification algorithm was assessed, and the average relative error was reduced by over 38%. It indicates that the differences of the backscattering properties in different time and space are converted into the differences of bio-optical properties of dominant factors in water.

REFERENCES

Ahn Y H, Bricaud A and Morel A. 1992. Light backscattering efficiency and related properties of some phytoplankters. Deep-Sea Research, 39(11-12): 1835–1855

Forget P, Broche P and Naudin J J. 2001. Reflectance sensitivity to solid suspended sediment stratification in coastal water and inversion: a case study. Remote Sensing of Environment, 77(1): 92–103

Huang C C, Li Y M, Wang Q, Sun D Y, Le C F, Wu L, Wang L Z and Wang X. 2009. Scattering characteristics and relevant factors in autumn Lake Taihu. Journal of Lake Sciences, 21(4): 594–602

Le C F, Li Y M, Zha Y, Sun D Y and Lv H. 2009. Simulation of backscattering properties of Taihu Lake. Advances in Water Science, 20(5): 707–713

Lee Z P, Carder K L and Arnone R A. 2002. Deriving inherent optical properties from water color: a multiband quasi-analytical algorithm for optically deep waters. Applied Optical, 41(27): 5755–5772

Li J S, Zhang B, Zhang X, Shen Q and Zhang Y L. 2008. A method of calculating back-scattering coefficients of suspended matter in water. Journal of Remote Sensing, 12(2): 193–198

Ma R H, Song Q J, Li G Y and Pan D L. 2008. Estimation of backscattering probability of Lake Taihu waters. Journal of Lake Sciences, 20(3): 375–379

Morel A, Gentili B, Chami M and Ras J. 2006. Bio-optical properties of high chlorophyll Case 1 waters and of yellow-substance-dominated Case 2 waters. Deep-sea Research I, 53(9): 1439–1459

Morel A and Maritorena S. 2001. Bio-optical properties of oceanic waters: a reappraisal. Journal of Geophysical Research, 106(C4): 7163–7180

Shi K, Li Y M, Lv H, Sun D Y, Huang C C, Wang Y F and Jin X. 2010. Depth profile of suspended particle scattering coefficient and its impact factors in Taihu Lake. Environmental Science, 31(3): 598–605

Song Q J and Tang J W. 2006. The study on the scattering properties in the Huanghai Sea and East China Sea. Acta Oceanologica Sinica, 28(4): 56–63

Stramska M, Stramski D, Hapter R, Kaczmarek S and Stoń J. 2003. Bio-optical relationships and ocean color algorithms for the north polar region of the Atlantic. Journal of Geophysical Research, 108(C5): 3143

Stramski D, Boss E, Bogucki D, Kenneth J and Voss K J. 2004. The role of seawater constituents in light backscattering in the ocean. Progress in Oceanography, 61(1): 27–56

Stramski D, Bricaud A and Morel A. 2001. Modeling the inherent optical properties of the ocean based on the detailed composition of the planktonic community. Applied Optics, 40(18): 2929–2945

Sun D Y, Li Y M, Le C F, Gong S Q, Wang H J, Wu L and Huang C C. 2007. Scattering characteristic of Taihu Lake and its relationship models with suspended particle concentration. Chinese Journal of Environmental Science, 28(12): 2688–2694

Sun D Y, Li Y M, Wang Q, Le C F, Huang C C and Wu L. 2008. The scattering characteristics of Lake Taihu waters. Journal of Lake Sciences, 20(3): 389–395

Tang J W, Tian G L, Wang X Y, Wang X M and Song Q J. 2004. The methods of water spectra measurement and analysis: I Above-water method. Journal of Remote Sensing, 8(1): 37–44

Tzortziou M, Herman J R, Gallegos C L, Neale P J, Subramaniam A, Harding L W and Ahmad Z. 2006. Bio-optics of the Chesapeake Bay from measurements and radiative transfer closure. Estuarine, Coastal and Shelf Science, 68(1-2): 348–362

Zhang Y L, Qin B Q, Chen W M, Hu W P, Gao G, Zhu G W and Luo L C. 2005. Attenuation of photosynthetically available radiation (PAR) in Meiliang Bay under different winds and waves. Chinese Journal of Applied Ecology, 16(6): 1133–1137

Zhang Y L, Zhang B, Wang X, Li J S, Feng S, Zhao Q H, Liu M L and Qin B Q. 2007. A study of absorption characteristics of chromophoric dissolved organic matter and particles in Lake Taihu, China. Hydrobiologia, 592(1): 105–120

基于光谱分类的太湖水体后向散射研究

陆超平，吕恒，李云梅

南京师范大学 虚拟地理环境教育部重点实验室，江苏 南京 210046

摘　要：由于时空变化而产生的水体后向散射系数参数化差异一直是影响水质参数遥感定量反演精度的一个重要因素。在对太湖遥感反射率光谱进行分类的基础上，针对影响太湖水体水色的不同主导因子，把太湖水体分为3种类型，分别利用半分析方法和光学闭合原理对后向散射系数进行模拟，在此基础上研究其光学特性及其与水体组分浓度的关系，最后针对3种不同主导类型的水体分别建立了后向散射系数参数化模型。将后向散射特性在不同时间和空间上的差异转化为水体不同主导因子在生物-光学上的差异，从而得到适用于太湖不同湖区及不同季节的后向散射系数参数化模型，为利用分析方法对太湖水质参数进行更为精确的遥感反演提供了基础。

关键词：太湖，光谱分类，半分析方法，光学闭合原理，后向散射系数

中图分类号：X87　　　**文献标志码**：A

引用格式：陆超平，吕恒，李云梅．2012．基于光谱分类的太湖水体后向散射研究．遥感学报，16(2): 417–434
Lu C P, Lv H and Li Y M. 2012. Backscattering properties and parametric model of Taihu Lake based on spectral classification. Journal of Remote Sensing, 16(2): 417–434

1　引　言

光在水体传输过程中，会受到悬浮物、叶绿素和有色可溶性有机物(CDOM)的吸收和散射的影响。吸收系数和散射系数是衡量水体各组分对光照的吸收和散射程度的物理量，是水体重要的固有光学特性，其中后向散射部分的光线穿透水面形成离水辐亮度，是遥感传感器获取水体信息的来源和物理基础，是生物光学模型的重要输入参数(Forget 等，2001；Stramski 等，2004)，因此，对水体后向散射特性的研究是生物光学模型建立的基础。

现有专门针对水体后向散射光学特性的研究相对较少，且主要针对光学特性受浮游藻类主导的海洋一类水体进行(Stramski 等，2001；Morel和Maritorena，2001；Stramska 等，2003)。宋庆君和唐军武(2006)通过AC9和HS6实测水体吸收和后向散射对黄东海近海岸水体颗粒物后向散射光谱特征进行了研究；孙德勇等人(2007，2008)通过AC-S、bb9对太湖水体散射特性及其与悬浮物浓度关系进行了研究；乐成峰等人(2009)基于辐射传输理论对太湖水体后向散射系数进行了模拟，并研究分析了其特性；马荣华等人(2008)对太湖水体的后向散射概率进行了研究；黄昌春等人(2009)对太湖水体秋季散射特性及其相关因素进行了分析；施坤等人(2010)对太湖水体颗粒物散射的剖面分布及其影响因素进行了分析。以上研究结果表明近岸水体以及湖泊水体的后向散射系数具有明显的时空差异性，即使对于同一个湖区，不同的季节，其后向散射参数化也存在较大差异。从生物-光学上分析，水体在不同时空上的光学差异，主要是源于水体组分的相互关系不同，如藻类和非藻类颗粒物的混合比例不同，即有些水体是藻类占主导作用，有些水体是非藻类颗粒物占主导作用，或者是两者共同主导。因此，有必要对水体主导因子进行深入研究，以寻求统一的模型对不同时间和空间后向散射系数进行参数化，从而更为准确地定量化表达水体光学特性，为水质参数遥感反演奠定基础。

收稿日期：2011-02-21；**修订日期**：2011-04-18

基金项目：国家自然科学基金(编号: 40701136，40971215)；国家水环境遥感技术体系研究与示范(编号: 2009ZX07527-006)；江苏高校优势学科建设工程资助项目

第一作者简介：陆超平(1987—　)，男，硕士研究生，专业是地图学与地理信息系统。E-mail: coollcp@126.com。

通信作者简介：吕恒(1977—　)，男，博士，副教授，研究领域为环境遥感。已发表学术论文十余篇。E-mail: HengLu@njnu.edu.cn。

本文首先对太湖2008年11月、2009年4月、2010年5月和2010年8月所有反射率光谱数据，按照不同主导因子水体在反射率光谱上的特征进行分类，然后分别结合Lee等人(2002)提出的基于生物光学模型的半分析方法和Tzortziou等人(2006)利用的光学闭合原理，通过对半分析模型中经验参数的调整和利用光学闭合原理进行误差控制，模拟太湖水体后向散射系数，在此基础上对太湖不同类别水体后向散射系数的特性及其与悬浮物浓度的关系进行研究，并对各类别水体后向散射系数分别进行参数化表达，以期将后向散射特性在不同时间和空间上的差异转化为水体不同主导因子在生物-光学上的差异，从而得到适用于不同时间和空间尺度的后向散射系数参数化模型，为利用分析方法对太湖水质参数进行更为精确的遥感反演提供依据。

2 材料与方法

2008年11月、2009年4月、2010年5月和2010年8月对太湖共采集测量了184条数据，点位分布如图1所示。测量的参数包括水体遥感反射率、水体中总悬浮物浓度、有机悬浮物浓度、无机悬浮物浓度、黄质的吸收系数、叶绿素浓度以及色素颗粒物的吸收系数。其中，遥感反射率在野外直接观测，总悬浮物浓度、有机悬浮物浓度、黄质的吸收系数、无机悬浮物浓度、叶绿素浓度、色素颗粒物的吸收系数和总悬浮物的吸收系数等参数通过室内分析获取。

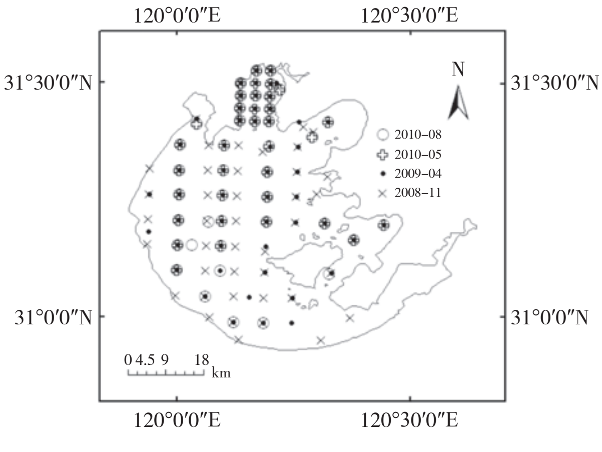

图1 太湖采样点位分布图

2.1 参数的测定

光谱测试使用由美国分析光谱仪器公司(Analytical Spectral Devices)制造的ASD野外光谱辐射仪(ASD Field Spec)。光谱采集和处理的方法采用唐军武等人(2004)提出的水面以上测量法。每个采样点测量10次光谱。进行遥感反射比计算时，先对测得的光谱数据进行异常数据剔除，去除数值较高的光谱曲线，保留数据较低的光谱曲线进行平均。然后将平均处理后的数据代入文献(唐军武 等，2004)的公式，得到水体的离水辐亮度和遥感反射比。在计算遥感反射比时，根据测量时的天气状况，气-水界面对天空光的反射比r取0.025；选用经过严格定标的30 %的灰板。π取3.1415926。

水体的总吸收包括黄质吸收、悬浮颗粒物吸收和纯水吸收。CDOM的吸收系数采用比色皿测量，悬浮颗粒物的吸收采用定量滤膜技术(QFT)测定，叶绿素浓度测定采用“热乙醇法”，悬浮物浓度采用“称重法”测定(Zhang 等，2007)。

2.2 基于遥感反射率光谱的分类

根据太湖水体遥感反射率曲线的波谱特征结合影响遥感反射率的水体水质参数的组成，本文把太湖水体分为以藻类颗粒物为主导(类型一)、藻类与非藻类共同主导(类型二)以及由非藻类颗粒物主导的水体类型(类型三)。不同类型的遥感反射率对应不同的固有光学-生物特性，由藻类主导的水体在反射率光谱上会更多的表现出藻类的特征，比如675 nm处的吸收峰和700 nm处的反射峰；由非藻类颗粒物主导的水体和藻类与非藻类共同主导的水体在反射率光谱上会表现出各自的特征。所以，通过对水体遥感反射率光谱的分类，可以有效地将水体分为不同主导因子的水体。

类型一中，色素颗粒物的吸收作用较强，而悬浮物的散射作用相对较弱，在675 nm处呈现明显的吸收峰，700 nm左右出现明显的反射峰；类型三中，由于高浓度悬浮物对叶绿素信息的掩盖，导致色素颗粒物在675 nm处的吸收特性和700 nm左右的荧光特性在反射率光谱上的谷峰形状基本消失，且在570 nm处的反射峰比类型一的平缓；类型二中，既含有一定的藻类的反射率峰谷特性，也包含了非藻类颗粒物的散射特性。

通过对570 nm附近反射峰的左半峰的斜率进行统计分析，发现斜率值0.00015可以作为类型一和其他两种类型的分类标准之一；而700 nm附近的反射峰与675 nm附近的反射谷之间的斜率可以对3种类型进行一定的区分。所以，结合这两个判断标准可以对3种不同类型的遥感反射率进行分类。由于各遥感反射率光谱曲线的峰谷位置会有偏移，所以采用算法1对其进行自动搜索分类，算法流程如图2所示。

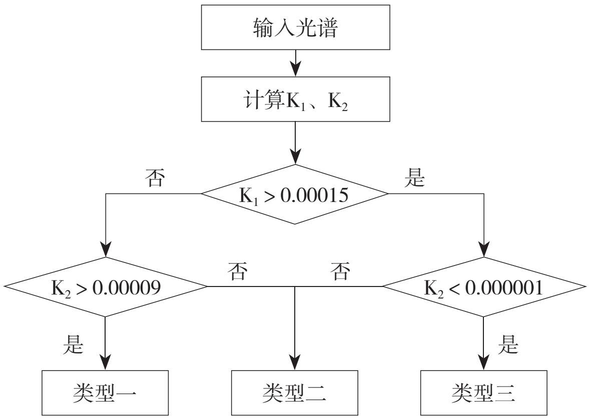

图2　基于遥感反射率的自动搜索分类算法

$K_1=[\mathrm{peak}(R_{rs}(\lambda_1))-R_{rs}(\lambda_1-40)]/40$，$(540<\lambda_1<600)$，表示570 nm附近反射峰的左半峰的斜率；$R_{rs}$表示遥感反射率。
$K_2=[\mathrm{peak}(R_{rs}(\lambda_2))-\mathrm{valley}(R_{rs}(\lambda_3))]/(\lambda_2-\lambda_3)$，$(670<\lambda_2<730，620<\lambda_3<680)$，表示700 nm附近的反射峰与675 nm附近的反射谷之间的斜率；peak()和valley()函数分别自动搜索给定范围内的反射峰与反射谷)

2.3　后向散射及吸收模拟

利用Lee等人(2002)提出的QAA算法以遥感反射率为输入计算样点的后向散射系数和吸收系数。Lee在QAA算法中对参考波长λ_0的选择及$a(\lambda_0)$的经验公式是针对特定研究区域建立的，而对于太湖而言目前尚没有适合的类似的经验公式。从已有的研究结果来看，700 nm之后水体的总吸收可以认为主要是纯水的吸收，所以本文采用迭代的方式选取最优的参考波长，迭代区间为700—730 nm。同理，从已有的对太湖Y值(Y是参数化模型的指数，表示后向散射系数随波长增加而衰减的速率。)的研究结果来看(孙德勇 等，2007，2008；乐成峰 等，2009)，不同的研究区域，Y值在0—3之间变化，所以Y值也通过迭代得到。g_0和g_1的取值引用Lee在QAA算法中针对高散射水体的取值，分别为0. 084和0. 17。

利用光学闭合原理，可以模拟得到参考波长λ_0，并计算得到$b_{bp}(\lambda)$和水体总吸收系数$a(\lambda)$，具体方法见算法2：

步骤 1　设定参考波长λ_0初始值为700 nm；

步骤 2　设置Y的值在0—3之间以0.1为步长进行迭代，通过表1中的计算步骤，得到水体总后向散射系数$b_{bp}(\lambda)$和水体总吸收系数$a(\lambda)$；

步骤 3　计算模拟得到的$a(\lambda)$与实测总吸收在可见光波段范围的平均相对误差，若误差小于10%(Tzortziou 等，2006)，则记录下λ_0、Y值、$b_{bp}(\lambda)$和误差值；否则该采样点被认为是异常点剔除；

步骤 4　如果，λ_0小于730 nm，将λ_0增加1 nm，转入**步骤 2**；否则转入**步骤 5**；

步骤 5　将记录下来的误差值，针对不同λ_0分别求平均误差，将平均误差最小的λ_0作为参考波长。

表1　半分析方法具体步骤及公式

步骤	变量	公式	方法类型
0	r_{rs}	$=R_{rs}/(0.52+1.7R_{rs})$	半分析模型
1	$u(\lambda)$	$=\dfrac{-g_0+[(g_0)^2+4g_1r_{rs}]^{1/2}}{2g_1}$	半分析模型
2	$a(\lambda_0)$	$=a_w(\lambda_0)$，λ_0在700—730之间变化	逐步迭代
3	$b_{bp}(\lambda_0)$	$=\dfrac{u(\lambda_0)a(\lambda_0)}{1-u(\lambda_0)}-b_{bw}(\lambda_0)$	分析模型
4	Y	0—3之间变化	逐步迭代
5	$b_{bp}(\lambda)$	$=b_{bp}(\lambda_0)\left[\dfrac{\lambda_0}{\lambda}\right]^Y$	半分析模型
6	$a(\lambda)$	$=\dfrac{[1-u(\lambda)][b_{bw}(\lambda)+b_{bp}(\lambda)]}{u(\lambda)}$	分析模型

注：r_{rs}是水面以下辐照度比；b_{bp}为颗粒物后向散射系数；b_{bw}为纯水的后向散射系数

3　结果与分析

3.1　基于遥感反射率光谱的分类

利用算法1对光谱数据进行分类，得到了3种不同主导类型水体的光谱，分别为藻类主导型水体的光谱、藻类与非藻类共同主导型水体的光谱和非藻类颗粒物主导型水体的光谱，分别对应类型一(图3)、类型二(图4)和类型三(图5)。图6显示了3种类型遥感反射率的平均值。可以看出，3种不同类型水体的遥感

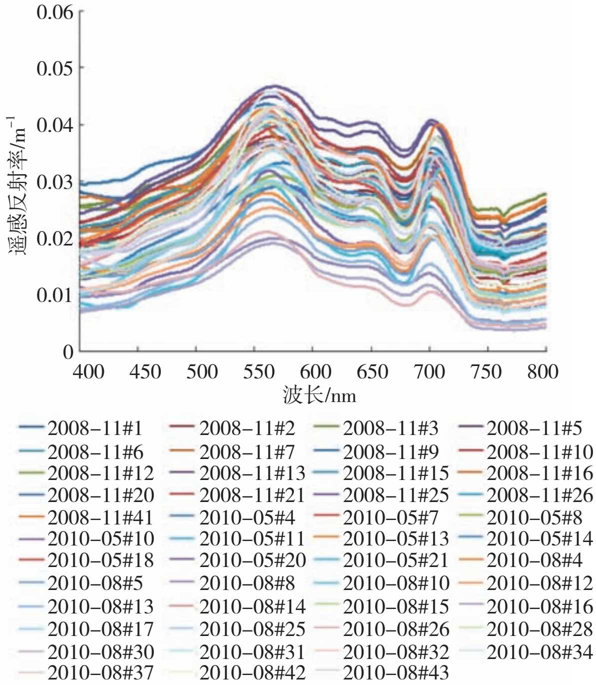

图3 类型一遥感反射率光谱曲线

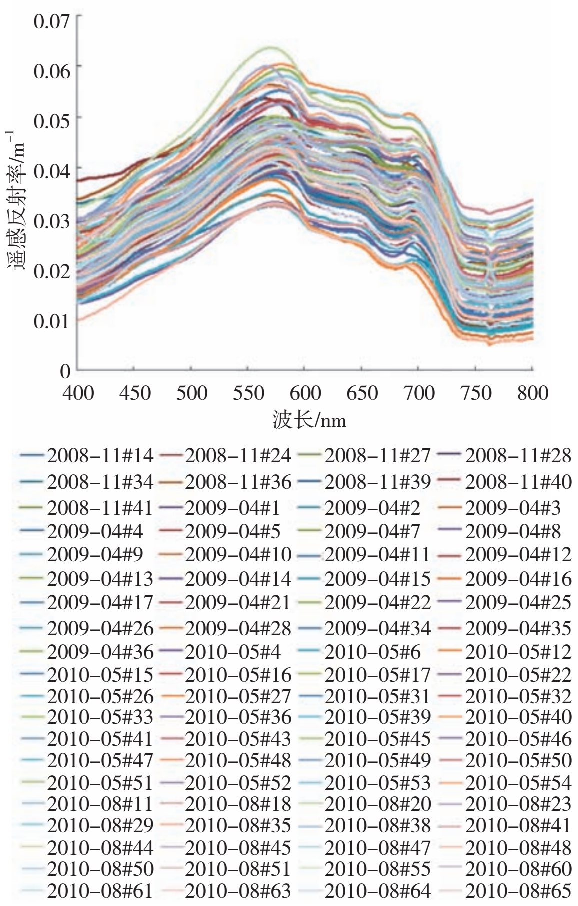

图4 类型二遥感反射率光谱曲线

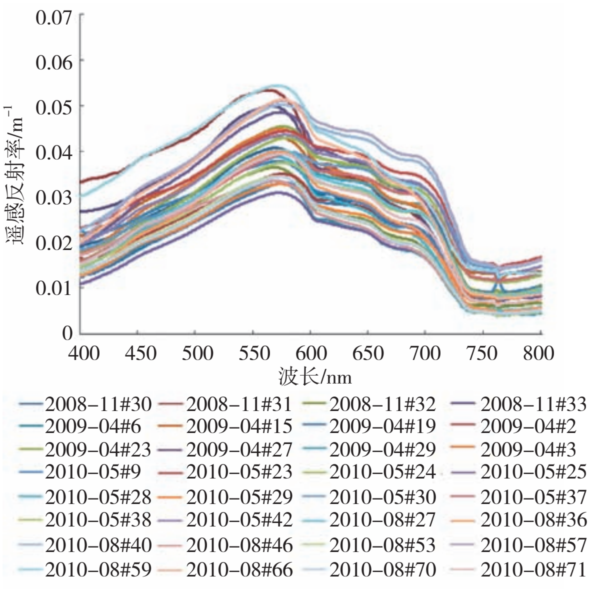

图5 类型三遥感反射率光谱曲线

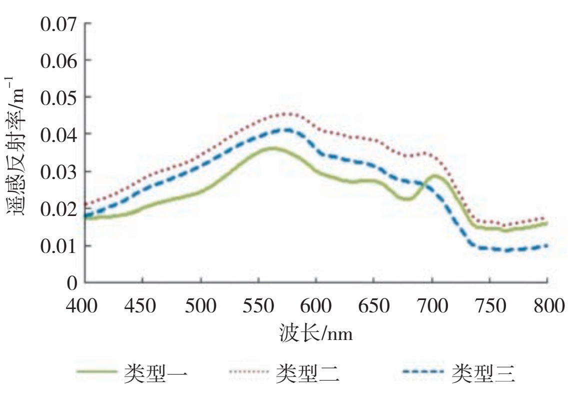

图6 3类遥感反射率的平均值

反射率特征比较明显，但光谱的不同类别是否能与水体的实际生物物理特性相吻合是该分类方法是否有效的判断依据。

表2给出了各类型遥感反射率对应的生物-光学特性。类型一具有较低的遥感反射率(图3、图6)，由藻类叶绿素和胡萝卜素的弱吸收和细胞的散射作用形成的反射峰出现在565 nm左右；由叶绿素a的荧光作用而产生的荧光峰出现在700 nm左右，两处反射率峰都较为明显；由藻类叶绿素在红光波段处的强吸收而形成的680 nm附近的吸收峰也较为明显；由表2可知类型一水体的叶绿素浓度、有机悬浮物浓度和色素颗粒物在675 nm处的吸收系数分别为44. 06 mg/m^3、16.47 mg/L和0.88 m^{-1}，明显大于类型二和类型三的平均值。无机悬浮物与总悬浮物比值的平均值为0.55，明显小于类型二和类型三的平均值。类型一的样点共计60个，占总样点的32.6%，主要分布在太湖梅梁湾及周边湖区叶绿素浓度较高而总悬浮物浓度相对较低的水体。可见，类型一水体的光学特性主要是由浮游藻类主导的。

表2 不同类型水体的生物光学量

光学及生物量	平均值		
	类型一	类型二	类型三
TSM/(mg/L)	37.58	60.78	72.93
OSM/(mg/L)	16.47	10.27	11.25
ISM/(mg/L)	21.11	50.51	61.69
ISM/TSM	0.55	0.78	0.85
Chl_a/(mg/m^3)	44.06	17.14	8.08
aph(675)/(m^{-1})	0.88	0.35	0.21

在类型三(图4、图6)中，由藻类色素引起的两处反射峰不明显，由藻类叶绿素和胡萝卜素弱吸收和细胞的散射作用形成的反射峰出现在585 nm左右；由于叶绿素a的荧光作用而产生的荧光峰和由藻类叶绿素在红光波段处的强吸收而形成的吸收峰的峰谷特征已经基本被无机悬浮物掩盖；由表2可知总悬浮物浓度、无机悬浮物浓度和无机悬浮物与总悬浮物比值的平均值分别为72.93 mg/L、61.69 mg/L和0.85 mg/L；虽然总悬浮物的浓度不算太高，但无机悬浮物在总悬浮物中所占的比例很高，说明该类水体无机悬浮物起主导作用。类型三的色素颗粒物在675 nm处的吸收系数为0.21 m^{-1}，仅为类型一的四分之一，说明浮游藻类在类型三水体中的作用较小。类型三的样点共计41个，占总样点数的22.3%，主要分布在太湖湖心区域叶绿素浓度较低而总悬浮物浓度相对较高的水体。可知，类型三水体的光学特性主要是由悬浮物特别是非藻类悬浮物主导的。

在类型二(图5、图6)中，由藻类色素引起的两处反射峰不如类型一的明显，但比类型三的明显。由藻类叶绿素和胡萝卜素弱吸收和细胞的散射作用形成的反射峰出现在583 nm左右；由叶绿素a的荧光作用而产生的荧光峰出现在697 nm左右；由藻类叶绿素红光波段处的强吸收而形成的吸收峰出现在683 nm左右；由表2可知类型一的色素颗粒物在675 nm处的吸收系数、叶绿素浓度以及有机悬浮物占总悬浮物的比例的平均值分别为0.34 m^{-1}、17.14 mg/m^3、0.22，介于类型一和类型三之间。叶绿素浓度高于类型三，同时无机悬浮物占总悬浮物比例高于类型一，藻类与非藻类悬浮物共同作用于水体。类型二共计83个样点，占总样点的45.1%。可见，类型二水体的光学特性主要是由非藻类悬浮物和浮游藻类共同主导的。

3.2 不同类型水体后向散射系数及其特征

基于算法2对分类后的数据分别进行模拟计算，得到不同类型水体的参考波长λ_0，藻类颗粒物主导的参考波长为715 nm，藻类与非藻类混合主导的参考波长为710 nm，非藻类颗粒物主导的参考波长为706 nm。这个模拟结论与乐成峰等人(2009)认为的715 nm基本一致。参考波长从类型一、类型二和类型三依次向短波方向移动，说明在3种类型的水体中，随着藻类含量的减少，在700 nm以后，纯水吸收越来越近似等于水体总吸收。

图7、图8、图9分别给出了3种不同类型水体的后向散射系数光谱曲线。从图中可以看出，各采样点后向散射系数具有类似的光谱特征，随着波长向长波方向移动，后向散射系数呈指数递减，该结论与其他学者的研究结果相一致(孙德勇 等，2008；乐成峰 等，2009；黄昌春 等，2009)。由于不同采样点水体各组分的浓度差异，使得后向散射系数大小具有一定的差异性。类型一在400 nm处的后向散射系数$b_{bp}(400)$最大值为3.31 m^{-1}，最小值为0.32 m^{-1}，平均值为1.54 m^{-1}；在532 nm处后向散射系数$b_{bp}(532)$的变化

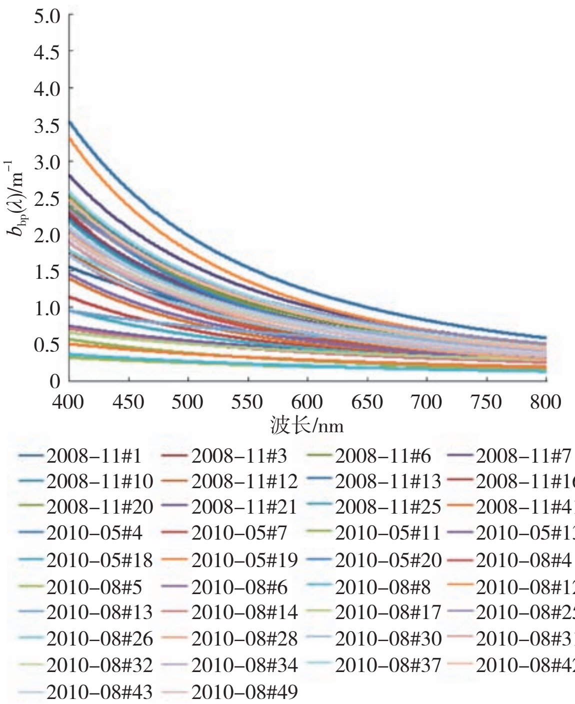

图7 类型一后向散射系数

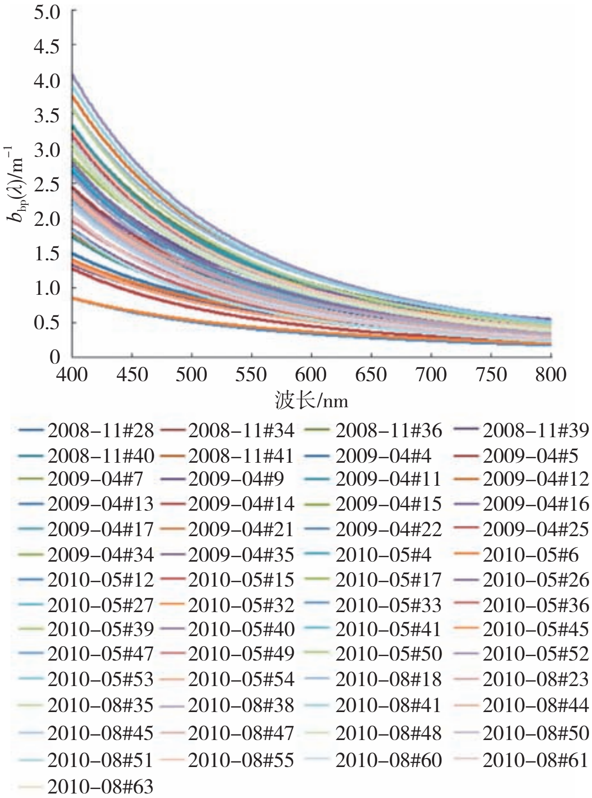

图8 类型二后向散射系数

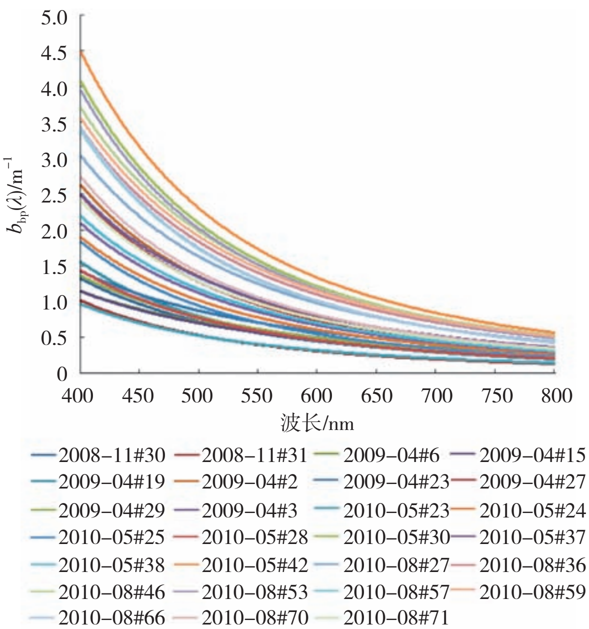

图9 类型三后向散射系数

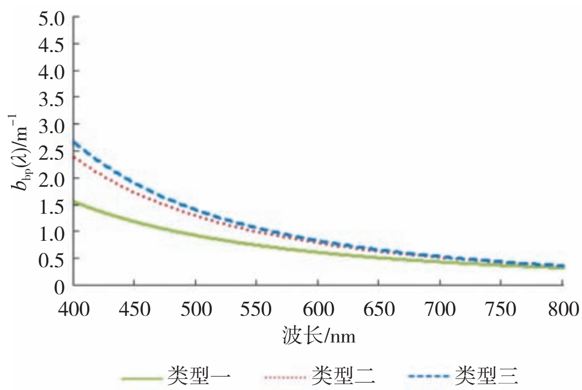

图10 3种类型后向散射系数平均值

范围为0.22—1.65 m^{-1}，平均值为0.74 m^{-1}；在675 nm处后向散射系数的变化范围相对较小，最大值为0.77 m^{-1}，最小值为0.18 m^{-1}，平均值为0.47 m^{-1}。类型二在400 nm、532 nm和675 nm处的后向散射系数变化范围分别为：0.85—4.07 m^{-1}，0.44—1.96 m^{-1}，0.28—0.85 m^{-1}。类型三在400 nm、532 nm和675 nm处的后向散射系数变化范围分别为：0.96—4.47 m^{-1}，0.41—1.92 m^{-1}，0.23—0.93 m^{-1}。图10为3种不同类型水体后向散射系数的平均值光谱曲线。从图10可以看出，3条曲线都呈指数递减趋势，但后向散射系数从类型三到类型一依次减小。这与Morel等人(2006)认为以藻类颗粒物主导的一类水体的后向散射要低于黄质控制的二类水体的结论相符。从400 nm到550 nm，类型一的后向散射系数递减的速度要明显小于类型二和类型三，类型二和类型三较为接近，仅在数值上略小于类型三；600 nm以后，3条曲线均趋于平缓。

3.3 不同类型水体后向散射系数与悬浮物浓度关系

为了研究水体中不同组分对后向散射系数的影响，将后向散射系数与总悬浮物、无机悬浮物浓度、有机悬浮物浓度及叶绿素含量进行相关性分析。

对于类型一，虽然是由藻类主导的水体，但在总悬浮物中无机悬浮物占有的比例仍然高于有机悬浮物(表2)，所以在表3中表现出，后向散射系数与无机悬浮物的相关系数要高于与有机悬浮物的相关系数，而后向散射系数与总悬浮物的相关系数最高。对于类型二，后向散射系数与总悬浮物的相关系数最高，而与无机悬浮物和总悬浮物的比值的相关系数最小，这恰恰说明了类型二水体是由藻类和非藻类颗粒物共同主导。对于类型三，后向散射系数与无机悬浮物的相关系数最高，这与类型三水体为非藻类颗粒物主导水体相一致。

表3 3种类型水体后向散射系数与水体组分浓度的相关系数

	TSM	ISM	OSM	Chla	ISM/TSM
类型一$b_{bp}(532)$	0.76	0.56	0.48	0.53	0.38
类型二$b_{bp}(532)$	0.80	0.65	0.37	0.21	0.19
类型三$b_{bp}(532)$	0.77	0.89	0.65	0.24	0.63

利用线性函数分别对3种类型水体的后向散射系数与TSM或ISM进行拟合，如图11、图12、图13所示，类型三水体的后向散射系数与无机悬浮物拟合效果最好，类型一水体的后向散射系数与总悬浮物拟合效果稍差。

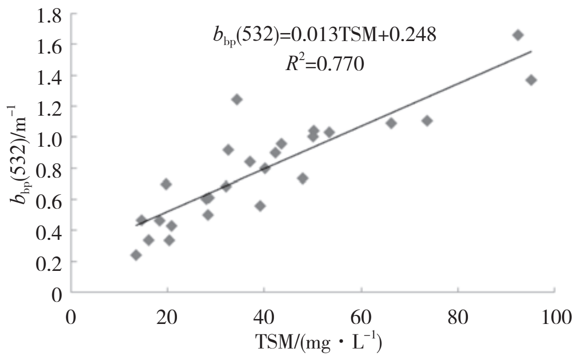

图11 类型一的532 nm后向散射系数与总悬浮物浓度的拟合曲线

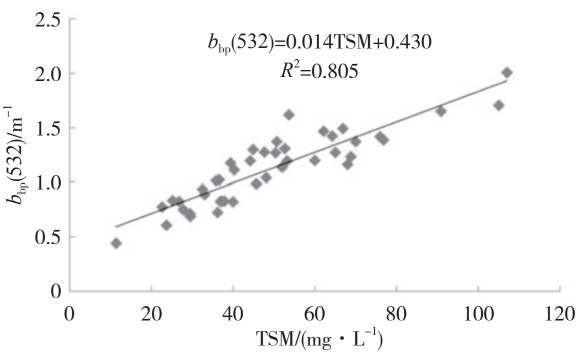

图12 类型二的532 nm后向散射系数与总悬浮物浓度的拟合曲线

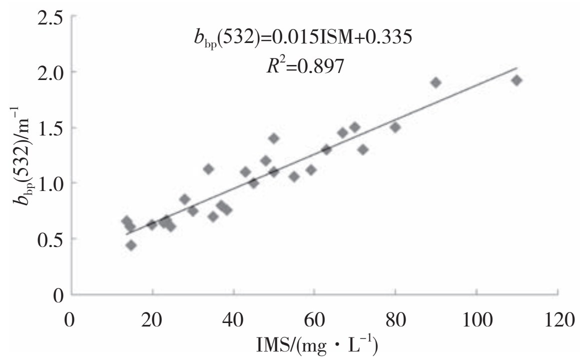

图13 类型三的532 nm后向散射系数与无机悬浮物浓度的拟合曲线

类型一的关系式为：

$$b_{bp}(532)=0.013\times \text{TSM}+0.248 \quad (1)$$

类型二的关系式为：

$$b_{bp}(532)=0.014\times TSM+0.430 \tag{2}$$

类型三的关系式为：

$$b_{bp}(532)=0.015\times ISM+0.335 \tag{3}$$

3.4　不同类型水体后向散射系数参数化

后向散射系数参数化能够使得整个波长范围的后向散射系数可以通过少数波段来表达，由此可以降低数据获取的难度，同时也减少实验数据获取中不确定性因素造成的误差。因此，在水质参数反演模型构建以及水体辐射传输模拟中，常常需要进行后向散射系数的参数化。目前通常采用指数模型对水体的后向散射系数进行参数化模拟(Stramska 等，2003；宋庆君和唐军武，2006)。

$$b_{bp}(\lambda)=b_{bp}(\lambda_0)\left[\frac{\lambda_0}{\lambda}\right]^n \tag{4}$$

式中，$b_{bp}(\lambda_0)$为参考波段λ_0处的后向散射系数；n为后向散射系数随波长变化的指数，与水体中悬浮物浓度及组成成分有关。

本研究以532 nm为参考波长，分别对3种类型水体的后向散射系数进行参数化。首先用后向散射系数$b_{bp}(\lambda)$与$b_{bp}(532)$进行线性拟合，拟合关系式为$b_{bp}(\lambda)=A(\lambda)\times b_{bp}(532)$，然后利用获得的系数值$A$与波长比值$\lambda_0/\lambda$进行幂函数拟合，分别得到类型一的指数$n$=2.12，类型二的指数$n$=2.51，类型三的指数$n$=2.69。最终得到3种类型水体的后向散射系数光谱模型，如式(5)(6)(7)。

类型一的后向散射系数光谱模型为：

$$b_{bp}(\lambda)=b_{bp}(532)\left[\frac{532}{\lambda}\right]^{2.12} \tag{5}$$

类型二的后向散射系数光谱模型为：

$$b_{bp}(\lambda)=b_{bp}(532)\left[\frac{532}{\lambda}\right]^{2.51} \tag{6}$$

类型三的后向散射系数光谱模型为：

$$b_{bp}(\lambda)=b_{bp}(532)\left[\frac{532}{\lambda}\right]^{2.69} \tag{7}$$

将式(1)、(2)、(3)分别代入式(5)、(6)、(7)，得到：

类型一：

$$b_{bp}(\lambda)=(0.013\times TSM+0.248)\left[\frac{532}{\lambda}\right]^{2.12} \tag{8}$$

类型二：

$$b_{bp}(\lambda)=(0.014\times TSM+0.430)\left[\frac{532}{\lambda}\right]^{2.51} \tag{9}$$

类型三：

$$b_{bp}(\lambda)=(0.015\times ISM+0.335)\left[\frac{532}{\lambda}\right]^{2.69} \tag{10}$$

诸多学者对不同水体中悬浮颗粒物后向散射系数光谱模型作过研究，如宋庆君和唐军武(2006)对黄东海海区后向散射特性研究时，得到的光谱模型的平均指数为1.146，变化范围为0.61—1.99；孙德勇等人(2007)对太湖水体研究时得到的指数为3.06；乐成峰等人(2009)对太湖研究时得到的指数为2.09，变化范围为1.32—2.8。孙德勇和乐成峰得到的指数n值差别较大，这主要是由于不同采样点以及不同采样时期，太湖水体组分和浓度都存在一定的差异性导致的。太湖为典型的大型浅水湖泊，由于水动力环境、外界环境等因素的变化导致其水体中悬浮物的浓度和组成都存在着较大的变化，风浪使得太湖底泥的再悬浮，导致水体中悬浮物浓度变化较大(张运林 等，2005)，从而造成每个人研究中的n值与其他研究者具有一定的差异。本研究中n值的变化范围介于孙德勇与乐成峰的之间，类型一的n值与乐成峰的较为接近，类型三的n值与孙德勇的较为接近，类型二的n值介于类型一和类型三之间。这恰恰说明了通过对水体分类来进行后向散射系数参数化可以有效克服时空差异及外界因素带来的参数波动。

3.5　分类效果验证

在后向散射系数模拟的半分析方法中，吸收系数是通过后向散射系数求得。所以，在没有实测的后向散射系数进行验证的情况下，本文通过对分类前后，吸收系数模拟值与实测值的误差分析，来衡量分类的效果。运用算法2分别对分类前后的数据进行模拟，结果见表4。可以看出，通过对不同主导因子的遥感反射率进行分类，再分别进行后向散射系数和吸收系

数的模拟，得到吸收系数模拟值与实测值的平均相对误差比不分类的减小38%以上。分类后的模拟精度得到较大提高。

表4 分类前后的模拟结果对比

	参考波长λ_0			吸收系数模拟值与实测值的平均相对误差/%			Y值		
分类前	710			11.7			2.54		
分类后	类型一	类型二	类型三	类型一	类型二	类型三	类型一	类型二	类型三
	715	710	706	6.5	7.3	6.1	2. 12	2. 51	2. 69

4 结论与讨论

利用辐射传输理论获取后向散射系数可以避免仪器操作过程中的人为因素和环境因素的影响，在水体固有光学特性的研究中具有一定的优势(Tzortziou 等，2006；李俊生 等，2008)。已有的研究基本都是对特定季节的研究，对于不同的季节，模型参数各不相同，模型在季节上存在很大的局限性，得到的是针对整个研究区的模型参数，但事实上整个湖区的后向散射特性在空间上也有较大差异。本文通过对不同季节的全区域水体，根据不同生物-光学特性来进行分类，将后向散射特性在不同时间和空间上的差异转化为水体不同主导因子在生物-光学上的差异，从而一定程度上解决了模型在时间和空间上的局限性。

本文首先依据遥感反射率光谱特征对水体进行分类，然后针对每一类水体，利用半分析模型和光学闭合原理对其后向散射系数进行了模拟。利用计算得到的总吸收系数与实测值进行比较，具有很好的吻合性。3种类型在400—700 nm的平均相对误差分别为6.5%、7.3%和6.1%。不分类模拟的平均相对误差分别为11.7%。由此可见，利用半分析方法和光学闭合原理模拟的后向散射系数能够使太湖生物光学模型较好的闭合，数据具有很好的准确性，能够反映太湖水体颗粒物后向散射系数的光学特性，而经过分类后的模拟精度更高，对太湖水体颗粒物后向散射系数的光学特性的反映更具有准确性。

(1) 在分析水体生物-光学特性和遥感反射率光谱特征的基础上，将太湖水体的反射率光谱分为藻类主导型水体光谱、藻类与非藻类共同主导型水体光谱和非藻类颗粒物主导型水体光谱。并对比分析了不同类别的生物-光学特性，结果表明基于遥感反射率光谱分类与水体的实际生物物理特性相吻合，可以有效的区分太湖的不同水体类型。

(2) Lee等人(2002)认为，随着水体的浑浊程度加大，参考波段λ_0的选择需要向长波方向移动从而获得更好的反演效果，但不宜过大，因为随着波段变大，遥感反射率变小，从而误差会变大。本文根据太湖水体在715 nm附近的吸收主要由纯水主导的特性，选择700—730 nm作为迭代范围进行自动迭代筛选，分别得到715 nm、710 nm、706 nm作为3种类型水体的半分析模型中的参考波段，对太湖水体后向散射系数进行模拟。从计算得到的吸收系数与实测吸收系数的吻合度可以看出，算法显著提高了后向散射系数的模拟精度。

(3) 以532 nm为参考波段对3种类型的后向散射系数分别进行参数化，得出后向散射系数随波长变化的指数分别为：藻类颗粒物主导的指数为2.12，混合主导的指数为2.51，非藻类颗粒物主导的指数为2.69。最终得到3种类型水体的后向散射系数光谱模型。

(4) 对分类前后的模拟精度进行了比较，结果基于光谱分类的后向散射模拟精度提高了38%以上，说明通过将后向散射特性在不同时间和空间上的差异转化为水体不同主导因子在生物-光学上的差异，在一定程度上解决了由时空变化而产生的水体后向散射系数参数化差异的问题。

参考文献(References)

Ahn Y H, Bricaud A and Morel A. 1992. Light backscattering efficiency and related properties of some phytoplankters. Deep-Sea Research, 39(11-12): 1835–1855

Forget P, Broche P and Naudin J J. 2001. Reflectance sensitivity to solid suspended sediment stratification in coastal water and inversion: a case study. Remote Sensing of Environment, 77(1): 92–103

黄昌春, 李云梅, 王桥, 孙德勇, 乐成峰, 伍蓝, 王利珍, 王鑫. 2009. 太湖水体秋季散射特性及其相关因素分析. 湖泊科学, 21(4): 594–602

乐成峰, 李云梅, 查勇, 孙德勇, 吕恒. 2009. 太湖水体后向散射特性模拟. 水科学进展, 20(5): 707–713

Lee Z P, Carder K L and Arnone R A. 2002. Deriving inherent optical properties from water color: a multiband quasi-analytical algorithm for optically deep waters. Applied Optical, 41(27): 5755–5772

李俊生, 张兵, 张霞, 申茜, 张运林. 2008. 一种计算水体中悬浮物后向散射系数的方法. 遥感学报, 12 (2): 193–198

马荣华, 宋庆君, 李国砚, 潘德炉. 2008. 太湖水体的后向散射概率. 湖泊科学, 20(3): 375–379

Morel A, Gentili B, Chami M and Ras J. 2006. Bio-optical properties of high chlorophyll Case 1 waters and of yellow-substance-dominated Case 2 waters. Deep-sea Research I, 53(9): 1439–1459

Morel A and Maritorena S. 2001. Bio-optical properties of oceanic waters: a reappraisal. Journal of Geophysical Research, 106(C4): 7163–7180

施坤, 李云梅, 吕恒, 孙德勇, 黄昌春, 王彦飞, 金鑫. 2010. 太湖水体颗粒物散射的剖面分布及其影响因素分析. 环境科学, 31(3): 598–605

宋庆君, 唐军武. 2006. 黄海、东海海区水体散射特性研究. 海洋学报, 28(4): 56–63

Stramska M, Stramski D, Hapter R, Kaczmarek S and Stoń J. 2003. Bio-optical relationships and ocean color algorithms for the north polar region of the Atlantic. Journal of Geophysical Research, 108(C5): 3143

Stramski D, Boss E, Bogucki D, Kenneth J and Voss K J. 2004. The role of seawater constituents in light backscattering in the ocean. Progress in Oceanography, 61(1): 27–56

Stramski D, Bricaud A and Morel A. 2001. Modeling the inherent optical properties of the ocean based on the detailed composition of the planktonic community. Applied Optics, 40(18): 2929–2945

孙德勇, 李云梅, 乐成峰, 龚绍琦, 王海君, 伍蓝, 黄昌春. 2007. 太湖水体散射特性及其与悬浮物浓度关系模型. 环境科学, 28(12): 2688–2694

孙德勇, 李云梅, 王桥, 乐成峰, 黄昌春, 伍蓝. 2008. 太湖水体散射特性及其空间分异. 湖泊科学, 20(3): 389–395

唐军武, 田国良, 汪小勇, 王晓梅, 宋庆君. 2004. 水体光谱测量与分析: Ⅰ水面以上测量法. 遥感学报, 8(1): 37–44

Tzortziou M, Herman J R, Gallegos C L, Neale P J, Subramaniam A, Harding L W and Ahmad Z. 2006. Bio-optics of the Chesapeake Bay from measurements and radiative transfer closure. Estuarine, Coastal and Shelf Science, 68(1-2): 348–362

张运林, 秦伯强, 陈伟民, 胡维平, 高光, 朱广伟, 罗潋葱. 2005. 不同风浪条件下太湖梅梁湾光合有效辐射的衰减. 应用生态学报, 16(6): 1133–1137

Zhang Y L, Zhang B, Wang X, Li J S, Feng S, Zhao Q H, Liu M L and Qin B Q. 2007. A study of absorption characteristics of chromophoric dissolved organic matter and particles in Lake Taihu, China. Hydrobiologia, 592(1): 105–120